Mon. Not. R. Astron. Soc. **000**, 1–12 (2015) Printed 20 April 2015 (MN LaTeX style file v2.2)

Impact of weak interactions of free nucleons on the r-process in dynamical ejecta from neutron-star mergers

S. Goriely[1], A. Bauswein[2], O. Just[3,5], E. Pllumbi[3,4], and H.-Th. Janka[3]
[1] *Institut d'Astronomie et d'Astrophysique, Université Libre de Bruxelles, CP 226, 1050 Brussels, Belgium*
[2] *Department of Physics, Aristotle University of Thessaloniki, 54124 Thessaloniki, Greece*
[3] *Max-Planck-Institut für Astrophysik, Postfach 1317, 85741 Garching, Germany*
[4] *Physik Department, Technische Universität München, James-Franck-Straße 1, 85748 Garching, Germany*
[5] *Max-Planck/Princeton Center for Plasma Physics (MPPC)*

Released 2015 Xxxxx XX

ABSTRACT
We investigate β-interactions of free nucleons and their impact on the electron fraction (Y_e) and r-process nucleosynthesis in ejecta characteristic of binary neutron star mergers (BNSMs). For that we employ trajectories from a relativistic BNSM model to represent the density-temperature evolutions in our parametric study. In the high-density environment, positron captures decrease the neutron richness at the high temperatures predicted by the hydrodynamic simulation. Circumventing the complexities of modelling three-dimensional neutrino transport, (anti)neutrino captures are parameterized in terms of prescribed neutrino luminosities and mean energies, guided by published results and assumed as constant in time. Depending sensitively on the adopted ν_e-$\bar{\nu}_e$ luminosity ratio, neutrino processes increase Y_e to values between 0.25 and 0.40, still allowing for a successful r-process compatible with the observed solar abundance distribution and a significant fraction of the ejecta consisting of r-process nuclei. If the ν_e luminosities and mean energies are relatively large compared to the $\bar{\nu}_e$ properties, the mean Y_e might reach values >0.40 so that neutrino captures seriously compromise the success of the r-process. In this case, the r-abundances remain compatible with the solar distribution, but the total amount of ejected r-material is reduced to a few percent, because the production of iron-peak elements is favored. Proper neutrino physics, in particular also neutrino absorption, have to be included in BNSM simulations before final conclusions can be drawn concerning r-processing in this environment and concerning observational consequences like kilonovae, whose peak brightness and color temperature are sensitive to the composition-dependent opacity of the ejecta.

Key words: nuclear reactions, nucleosynthesis, abundances – neutrinos – stars: neutron – dense matter – hydrodynamics

1 INTRODUCTION

The r-process, or rapid neutron-capture process, of stellar nucleosynthesis is invoked to explain the production of the stable (and some long-lived radioactive) neutron-rich nuclides heavier than iron that are observed in stars of various metallicities, as well as in the solar system (for a review, see Arnould et al. 2007). Despite important effort to model potential r-process sites, all the proposed scenarios face serious problems and the site(s) of the r-process is (are) not identified yet. Until now, type-II supernovae or γ-ray bursts models have failed to provide convincing evidence for a successful r-processing that could significantly contribute to the Galactic enrichment in r-material (Wanajo et al. 2011; Janka 2012; Burrows 2013). Only magneto-rotational supernova explosions with extremely strong pre-collapse magnetic fields and fast rotation seem to provide favourable conditions for r-processing, but such rare events are not expected to be at the origin of the global galactic enrichment in r-process nuclei (Winteler et al. 2012; Nishimura et al. 2015; Wehmeyer et al. 2015).

For this reason, special attention is now being paid to neutron star (NS) mergers following the confirmation by hydrodynamic simulations that a significant amount of r-process enriched material, typically about 10^{-3} to a few $10^{-2} M_\odot$, can be ejected (Rosswog et al. 1999; Freiburghaus et al. 1999; Arnould et al. 2007; Metzger et al. 2010; Roberts et al. 2011; Goriely et al. 2011; Korobkin et al. 2012; Bauswein et al. 2013; Goriely et al. 2013; Wanajo et al. 2014;

Perego et al. 2014; Just et al. 2015; Sekiguchi et al. 2015). Recent nucleosynthesis calculations by Just et al. (2015) show that the combined contribution of both the dynamical (prompt) ejecta expelled during binary NS or NS-black hole (BH) mergers and the neutrino and viscously driven outflows generated during the post-merger remnant evolution of relic BH-torus systems can lead to the production of r-process elements from mass number $A \gtrsim 90$ up to thorium and uranium. The corresponding abundance distribution reproduces the solar distribution extremely well and can also account for the elemental distributions observed in low-metallicity stars (Roederer 2011; Roederer et al. 2012). Furthermore, recent studies (Matteucci et al. 2014; Komiya et al. 2014; Mennekens & Vanbeveren 2014; Shen et al. 2014; van de Voort et al. 2014; Vangioni et al. 2014; Wehmeyer et al. 2015) have reconsidered the galactic or cosmic chemical evolution of r-process elements in different evolutionary contexts. Although they do not converge towards one unique quantitative picture, most of them arrived at the conclusion that double compact star mergers may be the major production sites of r-process elements.

Despite the recent success of nucleosynthesis studies for NS mergers, the possibility of r-processing in these events is still affected by a variety of uncertainties. In particular, the impact of neutrino interactions is not yet studied and understood in detail, the main reason of which is the not yet manageable computational complexity associated with neutrino transport in a generically three-dimensional (3D), highly asymmetric environment with nearly relativistic fluid velocities and rapid changes in time. A computationally simple and much more efficient alternative to solving the time-dependent transport equation for neutrino distributions in the six-dimensional phase space is the use of a neutrino leakage scheme, in which the local neutrino net-emission (i.e., emission minus absorption) rate is estimated by a weighted interpolation between the pure emission rate and an optical-depth dependent diffusive loss term (e.g., Ruffert et al. 1996; Rosswog & Liebendörfer 2003). However, neutrino absorption cannot be straightforwardly included in a self-consistent manner in a leakage scheme because information about the local neutrino densities is missing in such a treatment.

It was long believed that neutrino interactions could not, at least not drastically, affect the initial neutron richness of the ejecta. Such expectations were based on numerical merger models. The temperatures of the merging NSs in these simulations, and therefore the neutrino production rates, remain low until the NSs collide with each other, and they rise in an increasing volume only gradually on a time scale of several milliseconds after the first contact of the two NSs (Ruffert & Janka 1999; Rosswog & Liebendörfer 2003; Wanajo et al. 2014). At this time a significant fraction of the ejecta material is already being expelled with nearly relativistic velocities. Newtonian merger studies suggested that a large part of the ejecta material even from symmetric mergers (i.e., for two equal-mass or close to equal-mass NSs) is thrown out by tidal forces in extended spiral arms forming from matter of the outer faces of the merging objects during their final approach and collision (Rosswog et al. 1999; Korobkin et al. 2012). By the tidal stretching these arms naturally remain unshocked and thus stay cool. Therefore they reach low densities so quickly that electron and positron captures cannot become efficient. Moreover, the ejecta escape to large radii before the neutrino emission of the compact merger remnant becomes sizable and neutrino absorption can affect the electron fraction significantly. Absorption of neutrinos radiated by the massive merger remnant is also diminished because the tidal ejection in Newtonian models happens preferentially in the orbital plane (see e.g. Rosswog et al. 1999; Korobkin et al. 2012) while the neutrinos are predominantly emitted perpendicular to this plane (Rosswog & Liebendörfer 2003; Dessart et al. 2009; Perego et al. 2014). However, the described situation applies well only for Newtonian mergers. The situation is different in the relativistic case.

Relativistic simulations of symmetric mergers do not show the development of prominent tidal arms, and the ejection of unshocked matter is therefore not important. Instead, the collision shock that builds up at the interface of the two NSs is typically stronger than in Newtonian conditions (see e.g. Bauswein et al. 2013), leading to potentially higher temperatures and higher, faster rising neutrino luminosities (Wanajo et al. 2014; Sekiguchi et al. 2015). The ejecta are expelled fairly spherically instead of equatorially (Bauswein et al. 2013; Hotokezaka et al. 2013) and consist of two main components, namely a first one in which very hot material is squeezed out from the collision interface of the two merging bodies, and a second, slightly delayed one that is expelled in waves from a torus-like belt of matter around the high-density core of the merger remnant. This torus is heated by spiral shocks that are sent out from the aspherical, wobbling, and rotating high-density core and that also lead to outward acceleration of parts of the torus matter (Bauswein et al. 2013; Hotokezaka et al. 2013; Just et al. 2015; Wanajo et al. 2014; Sekiguchi et al. 2015).

Indeed, recent relativistic NS-NS merger simulations that took into account neutrino emission by means of a leakage scheme and absorption by an additional approximate transport treatment based on a moment formalism (Wanajo et al. 2014; Sekiguchi et al. 2015), found that neutrino interactions with free nucleons can significantly increase the electron fraction in the dynamical ejecta for cases in which the collapse of the merger remnant to a black hole is delayed or does not happen. Under such conditions nuclei with mass numbers $A < 140$ can also be created in the dynamical ejecta in addition to the heavy r-process elements ($A > 140$). Weak interaction processes of free nucleons can consequently affect the strength of the r-process and the emerging abundance distribution.

The accurate inclusion of neutrino interactions in hydrodynamical simulations remains a highly complex task. This motivated us to conduct a simple, parametric study in order to quantify the potential impact of weak interactions on the electron-fraction evolution in merger ejecta and thus to explore the consequences of charged-current neutrino-nucleon reactions for the nucleosynthesis and possible r-processing in these ejecta. More specifically, we investigate the influence of β-interactions of electron neutrinos (ν_e) and electron antineutrinos ($\bar{\nu}_e$) with free n and p and of their inverse reactions,

$$\nu_e + n \rightleftharpoons p + e^- \tag{1}$$

$$\bar{\nu}_e + p \rightleftharpoons n + e^+ \quad , \tag{2}$$

on the Y_e distribution and r-process nucleosynthesis at conditions representative of the dynamical ejecta expelled by

hydrodynamical forces during NS-NS mergers. These reactions have been neglected in all previous studies of r-process nucleosynthesis for such ejecta except those of Wanajo et al. (2014), where their quantitative effects may depend on the adopted equation of state (Sekiguchi et al. 2015). The role of weak interactions for the electron fraction and the corresponding implications for r-process nucleosynthesis, however, demand further exploration in more detail, in particular also by basic, parametric modeling, because a multitude of uncertainties will prevent rigorous, self-consistent solutions of the full problem in the near future. Such uncertainties are associated with, for example, the extreme complexities of 3D energy-dependent neutrino transport in relativistic environments, with the neutrino opacities of dense, potentially highly magnetized matter, and with neutrino-flavor oscillations at rapidly time-variable, largely aspherical conditions of neutrino emission.

The main objective of our present work is a sensitivity study by the use of a parametric approach. It is intended to motivate further explorations of neutrino effects in relativistic NS-NS mergers in more detail and breadth. To this end, we set up a simplified and idealized theoretical framework to test the individual roles of the different weak interaction processes, considering the density and temperature evolution of fluid elements ejected from a prototype hydrodynamical, relativistic NS-NS merger model. For our parameter study we make assumptions about the neutrino emission properties that are guided by data taken from the literature. The electron fractions resulting from the neutrino-processing of the ejecta elements are then used as input for nuclear network calculations, allowing us to immediately link the effects of neutrino interactions to the final heavy-element production.

In Sect. 2 the employed merger model and our treatment of the weak neutrino reactions with free nucleons are described. The effects of β-processes on the electron fraction are reported in Sect. 3, and the subsequent r-process nucleosynthesis is analysed in Sect. 4. Conclusions are drawn in Sect. 5.

2 WEAK INTERACTIONS OF FREE NUCLEONS IN MERGER EJECTA

We adopt the density evolution of ejecta fluid elements from a representative NS-NS merger model, namely the symmetric $1.35M_\odot$-$1.35M_\odot$ binary model obtained with the temperature-dependent DD2 equation of state (Hempel & Schaffner-Bielich 2010; Typel et al. 2010) (essentially identical to the one in Bauswein et al. 2013, but with a higher resolution of $\sim 10^6$ particles). This relativistic hydrodynamic simulation also provides the temperature evolution. We do not apply any temperature post-processing as in Goriely et al. (2011) to disentangle temperature jumps in shocks from artificial heating associated with the use of a numerical viscosity in the smoothed-particle hydrodynamics scheme.

For each trajectory, we follow the expansion starting at a fiducial density of $\rho_{\rm eq} = 10^{12}\,{\rm g\,cm^{-3}}$, where we assume equilibrium to hold between electrons, positrons and neutrinos for the given total lepton number provided by our NS-NS merger model. Below $\rho_{\rm eq} = 10^{12}\,{\rm g\,cm^{-3}}$, electron, positron and electron neutrino and antineutrino captures are systematically included. Reactions of neutrinos on nuclei are, however, neglected. As long as the temperature remains in excess of typically $T > 10^{10}$ K, the abundance of heavy nuclei is determined by nuclear statistical equilibrium (NSE) at the given electron fraction, density and temperature. From the density $\rho_{\rm eq}$ down to the density $\rho_{\rm net}$, at which the temperature reaches 10 GK and the full reaction network is initiated, the β-interactions of free nucleons may affect the electron fraction Y_e. If a trajectory stays cooler than 10 GK below the density $\rho_{\rm eq}$, the network calculation is started at the neutron-drip density $\rho_{\rm drip}$, i.e., $\rho_{\rm net} = \rho_{\rm drip} \simeq 4.2\times10^{11}\,{\rm g\,cm^{-3}}$. The considered β-reactions involve free nucleons, whose abundance variations are given by

$$\begin{aligned} \frac{dY_n^{\rm f}}{dt} &= -\lambda_+ Y_n^{\rm f} + \lambda_- Y_p^{\rm f}\,, \\ \frac{dY_p^{\rm f}}{dt} &= \lambda_+ Y_n^{\rm f} - \lambda_- Y_p^{\rm f}\,, \end{aligned} \tag{3}$$

where $\lambda_+ = \lambda_{\nu_e} + \lambda_{e^+}$ and $\lambda_- = \lambda_{\bar\nu_e} + \lambda_{e^-}$. The λ_x denote capture rates of species $x \in \{e^-, e^+, \nu_e, \bar\nu_e\}$ onto free nucleons according to the β-reactions, Eqs. (1,2). The free neutron and proton numbers are related to Y_e by

$$\begin{aligned} Y_n^{\rm f} &= 1 - Y_e - \sum_{Z\geqslant 2} N\;Y(Z,N)\,, \\ Y_p^{\rm f} &= Y_e - \sum_{Z\geqslant 2} Z\;Y(Z,N)\,, \end{aligned} \tag{4}$$

where $Y = X/A$ is the molar fraction (and X the mass fraction) of the nucleus (Z,N) of atomic mass $A = Z+N$. Assuming that the NSE molar fractions of nuclei remain constant over the time step Δt, the time evolution of Y_e can be related to the change of the number of free protons, and written as

$$\frac{dY_e}{dt} = -\lambda_{\rm tot} Y_e + \lambda^*\,, \tag{5}$$

where $\lambda_{\rm tot} = \lambda_+ + \lambda_-$ and

$$\lambda^* = \lambda_+\left[1 - \sum_{Z\geqslant 2} NY\right] + \lambda_- \sum_{Z\geqslant 2} ZY\,. \tag{6}$$

If only free neutrons and protons are present, $\lambda^* = \lambda_+$. The impact of heavy nuclei is to increase λ^* towards λ_- (for matter made of α-particles only, $\lambda^* = \lambda_{\rm tot}/2$). The α-effect (McLaughlin et al. 1996; Meyer et al. 1998; Pllumbi et al. 2014), or more generally, the effect of heavy nuclei in binding neutrons and protons inside nuclei, is known to be responsible for driving Y_e towards 0.5 and is included in this term λ^*. If we assume that $\lambda_{\rm tot}$ and λ^* remain constant over the time step Δt (or, specifically, that Δt is chosen such that $\lambda_{\rm tot}$ and λ^* as well as the abundance of nuclei remain essentially constant during the time step), Eq. (5) can be integrated analytically leading to

$$Y_e(t+\Delta t) \simeq Y_e(t) e^{(-\lambda_{\rm tot}\Delta t)} + \frac{\lambda^*}{\lambda_{\rm tot}}\left[1 - e^{(-\lambda_{\rm tot}\Delta t)}\right]\,, \tag{7}$$

where $\lambda_{\rm tot}$ and λ^* are estimated at time t. This equation is used to follow Y_e from the initial density $\rho_{\rm eq}$ down to the density $\rho_{\rm net}$, at which the temperature has dropped to 10 GK (or, alternatively, to the drip density if temperatures above 10 GK are not reached for the considered trajectory).

For $t \gg 1/\lambda_{\rm tot}$, Y_e reaches the equilibrium value Y_e^∞

given by

$$Y_e^{\infty} \simeq \frac{\lambda^*}{\lambda_+ + \lambda_-} \simeq \frac{\lambda_{\nu_e} + \lambda_{e^+}}{\lambda_{\nu_e} + \lambda_{e^+} + \lambda_{\bar{\nu}_e} + \lambda_{e^-}} \quad . \tag{8}$$

The electron (anti)neutrino capture rates can be written in terms of the average (anti)neutrino capture cross sections $\langle\sigma_{\nu_e/\bar{\nu}_e}\rangle$ (Pllumbi et al. 2014) as

$$\lambda_{\nu_e} \simeq \frac{L_{\nu_e}}{4\pi r^2 \langle E_{\nu_e}\rangle}\langle\sigma_{\nu_e}\rangle\,, \tag{9}$$

$$\lambda_{\bar{\nu}_e} \simeq \frac{L_{\bar{\nu}_e}}{4\pi r^2 \langle E_{\bar{\nu}_e}\rangle}\langle\sigma_{\bar{\nu}_e}\rangle\,. \tag{10}$$

Here, the local (anti)neutrino number densities are expressed by the ratios of the global luminosities, $L_{\nu_e/\bar{\nu}_e}$, and the mean energies of the radiated neutrinos, $\langle E_{\nu_e/\bar{\nu}_e}\rangle$, multiplied with the spherical surface $4\pi r^2$ that surrounds the central neutrino source at a radial distance r (for every trajectory we adopt the time-dependent radial distance r from our hydrodynamical model). This r^{-2} dilution of the neutrino flux is a crude approximation and holds, at best, far away from the neutrinosphere, provided the emission is isotropic, i.e., if directional variations of the neutrino fluxes do not play a role. Close to and below the neutrinosphere, however, such a description breaks down but can be justified by the fact that at these locations electron and positron captures dominate and their competition enforces a state of weak equilibrium. At large distances the asymptotic electron fraction is determined by neutrino and antineutrino absorptions, for which reason direction-dependent differences of the neutrino exposure of the ejecta would be important for a detailed discussion of neutrino effects on merger ejecta. Nevertheless, despite these shortcomings, we apply the simple ansatz at all radii r where $\rho \leqslant \rho_{\rm eq}$ in order to discuss basic aspects of the impact of neutrino processes with nucleons in the merger ejecta in a parametric way.

Similar to Eqs. (9,10), the electron and positron capture rates are given in terms of the average electron/positron capture cross sections $\langle\sigma_{e^-/e^+}\rangle$ by

$$\lambda_{e^+} = c\,\tilde{n}_{e^+}\langle\sigma_{e^+}\rangle\,, \tag{11}$$

$$\lambda_{e^-} = c\,n_{e^-}\langle\sigma_{e^-}\rangle\,, \tag{12}$$

where c is the speed of light and n_{e^-} and $\tilde{n}_{e^+}$ the electron and positron densities, as detailed in Pllumbi et al. (2014).

In turn, the average cross sections for electron neutrino and antineutrino captures, as well as those for electron and positron captures, including the weak magnetism and recoil corrections, are taken from Pllumbi et al. (2014) (see also Horowitz & Li 1999). While the electron and positron capture rates are temperature- and density-dependent only, the (anti)neutrino capture rates depend on the (anti)neutrino luminosities and mean energies, hence require a detailed knowledge of the neutrino properties at each time step.

For the present study, we consider representative (anti)neutrino luminosities and angle-averaged mean energies that are assumed to remain constant in time. For a given mean energy $\langle E_{\nu_e}\rangle$, the electron neutrino temperature T_{ν_e} is deduced from the relation

$$\langle E_{\nu_e}\rangle = k_{\rm B} T_{\nu_e}\cdot\frac{F_3(0)}{F_2(0)} \quad , \tag{13}$$

where $k_{\rm B}$ is the Boltzmann constant and F_n are the fermi integrals (Takahashi et al. 1978) of order n for vanishing chemical potential, assuming nondegenerate neutrino spectra. A similar expression holds for the antineutrino temperature. For given (anti)neutrino luminosities and mean energies this allows us to determine all other moments of the (anti)neutrino energy spectra, and consequently the corresponding capture cross sections and rates (Eqs. 9,10).

Assuming that electron (anti)neutrino captures dominate over electron and positron captures and the abundance of heavy nuclei is negligible, the asymptotic value of Y_e (Eq. 8) can be approximated by

$$Y_e^{\nu\infty} \simeq \frac{L_{\nu_e}\varepsilon_{\nu_e} f^{\rm mr}_{\nu_e}}{L_{\nu_e}\varepsilon_{\nu_e} f^{\rm mr}_{\nu_e} + L_{\bar{\nu}_e}\varepsilon_{\bar{\nu}_e} f^{\rm mr}_{\bar{\nu}_e}}\,, \tag{14}$$

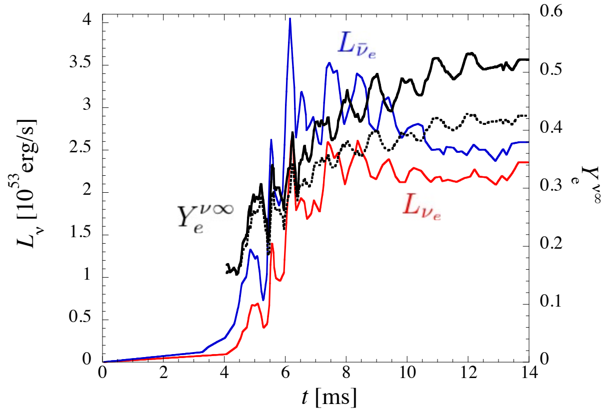

Figure 1. (Color online). Time evolution of the electron neutrino and antineutrino luminosities from Wanajo et al. (2014) and the corresponding $Y_e^{\nu\infty}$ (black solid line) as defined by Eq. (14). The black dotted line gives the $Y_e^{\nu\infty}$ without weak magnetism and recoil corrections, *i.e.* $f_\nu^{\rm mr} = 1$ in Eq. (14). The (anti)neutrino mean energies are taken consistently from Fig. 1 (lower panel) of Wanajo et al. (2014). Asymptotic values of $Y_e^{\nu\infty}$ are calculated only for non-negligible neutrino luminosities, *i.e.* for times $t \gtrsim 4$ ms.

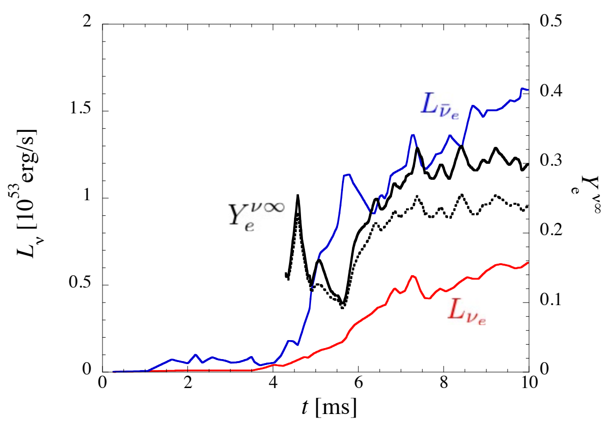

Figure 2. (Color online). Same as Fig. 1, but for the electron neutrino and antineutrino luminosities from Ruffert & Janka (2001). The (anti)neutrino mean energies are taken consistently from Fig. 17 (lower panel; Model Bc) of this reference.

because the rates can be expressed as $\lambda_\nu \propto L_\nu \varepsilon_\nu f_\nu^{\rm mr}$ ($\nu = \nu_e, \bar{\nu}_e$), where $\varepsilon_\nu = \langle E_\nu^2 \rangle / \langle E_\nu \rangle = F_4(0)F_2(0)/F_3^2(0) \times \langle E_\nu \rangle$ and $f_\nu^{\rm mr}$ corresponds to the weak magnetism and recoil corrections that can be found in Pllumbi et al. (2014). The corresponding value of $Y_e^{\nu\infty}$ is shown in Fig. 1 for the luminosities and mean energies of Wanajo et al. (2014) and lies between 0.25 and 0.50 for times $t \gtrsim 5\,{\rm ms}$ after the merging of the binary NSs. These values may, however, still be modified by effects of heavy nuclei. The weak magnetism and recoil corrections on the (anti)neutrino rates are seen in Fig. 1 to increase the asymptotic value of $Y_e^{\nu\infty}$ by up to 20% because they reduce the antineutrino capture cross section and simultaneously increase the neutrino capture cross section (Horowitz & Li 1999).

The neutrino properties, and in particular the antineutrino to neutrino luminosity ratio, are found to vary significantly between different hydrodynamical simulations but also depend on the adopted equation of state (Sekiguchi et al. 2015). Avoiding the complexity of self-consistent neutrino transport in hydrodynamical simulations, we shall restrict ourselves in our sensitivity study to constant luminosities and mean energies taken at selected times from previous simulations (Ruffert & Janka 2001; Wanajo et al. 2014). We consider first two representative sets of values for electron (anti)neutrino luminosities and mean energies as obtained by Wanajo et al. (2014) (see their Fig. 1), namely those corresponding to the instants of 5 and 6 ms, i.e.,

- Case 1: $t \simeq 5$ ms with $L_{\nu_e} = 0.6 \times 10^{53}$ erg/s; $L_{\bar{\nu}_e} = 1.3 \times 10^{53}$ erg/s; $\langle E_{\nu_e} \rangle = 12$ MeV; $\langle E_{\bar{\nu}_e} \rangle = 16$ MeV ,
- Case 2: $t \simeq 6$ ms with $L_{\nu_e} = 2.6 \times 10^{53}$ erg/s; $L_{\bar{\nu}_e} = 4.0 \times 10^{53}$ erg/s; $\langle E_{\nu_e} \rangle = 13$ MeV; $\langle E_{\bar{\nu}_e} \rangle = 16$ MeV .

Note that Case 1 leads to an asymptotic value $Y_e^{\nu\infty} \simeq 0.31$, whereas Case 2 yields $Y_e^{\nu\infty} \simeq 0.42$ (Fig. 1).

In order to test more thoroughly the impact of the neutrino processes on the nucleosynthesis, we also consider here the electron (anti)neutrino properties calculated in the NS merger simulation of Ruffert & Janka (2001) (cf Model Bc in their Fig. 17). The corresponding (anti)neutrino luminosities are shown in Fig. 2, together with the asymptotic values $Y_e^{\nu\infty}$ (with and without the weak magnetism and recoil corrections). Overall, lower luminosities are found in this model in comparison with Wanajo et al. (2014), but also a relatively higher emission of electron antineutrinos. Consequently, lower values of $Y_e^{\nu\infty}$ are predicted for this model. In our present sensitivity analysis we also select two cases for the electron (anti)neutrino luminosities and mean energies from the results of Ruffert & Janka (2001), namely those corresponding to times of 6 and 10 ms (and hereafter referred to as Cases 3 and 4, respectively), i.e.,

- Case 3: $t \simeq 6$ ms with $L_{\nu_e} = 0.3 \times 10^{53}$ erg/s; $L_{\bar{\nu}_e} = 10^{53}$ erg/s; $\langle E_{\nu_e} \rangle = 12.5$ MeV; $\langle E_{\bar{\nu}_e} \rangle = 17.4$ MeV ,
- Case 4: $t \simeq 10$ ms with $L_{\nu_e} = 0.6 \times 10^{53}$ erg/s; $L_{\bar{\nu}_e} = 1.6 \times 10^{53}$ erg/s; $\langle E_{\nu_e} \rangle = 13.5$ MeV; $\langle E_{\bar{\nu}_e} \rangle = 16.3$ MeV .

Case 3 leads to an asymptotic value $Y_e^{\nu\infty} \simeq 0.21$, while Case 4 yields $Y_e^{\nu\infty} \simeq 0.29$ (Fig. 2).

Finally, it should be mentioned that our assumption of time-independent (anti)neutrino luminosities can be questioned, since the neutrino-ejecta interaction is a highly time-dependent problem, where the relative time between the growth of the neutrino emission and the mass ejection matters. Considering constant luminosities is a very crude but simple approximation, which is sufficiently good to demonstrate the impact of neutrino processes on the time evolution and mass distribution of the electron fraction and the corresponding consequences for the r-process. A predictive assessment of neutrino effects on the nucleosynthesis in merger ejecta would also have to take account variations of the neutrino emission with different directions. Matter expelled towards the polar directions is exposed to different neutrino conditions than matter that leaves the system along equatorial trajectories. Again, a more detailed description of neutrino transport effects is demanded and is beyond the scope of our present parametric study.

3 IMPACT OF β-INTERACTIONS ON THE ELECTRON FRACTION

3.1 Time evolution of Y_e

To illustrate the impact of electron (anti)neutrino, electron and positron captures on the evolution of Y_e, we show in Figs. 3 and 4 the time evolution for two specific trajectories during the expansion from the initial density $\rho_{\rm eq} = 10^{12}\,{\rm g\,cm^{-3}}$ down to density $\rho_{\rm net}$, where the reaction network calculations are initiated. Both trajectories are studied including (anti)neutrino captures with neutrino properties for Case 1.

For trajectory 400720 (Fig. 3), neutrino and antineutrino captures on free nucleons with rates up to some $10^4\ {\rm s}^{-1}$ lead to a rapid increase of Y_e from 0.17 up to 0.31, corresponding to the asymptotic value of $Y_e^{\nu\infty}$ in Case 1. The (anti)neutrino rates are found to dominate the electron and positron capture rates already at densities slightly below $\rho_{\rm eq}$. This is linked to the slow $1/r^2$ decrease of the (anti)neutrino fluxes, which is more shallow than the steep temperature dependence (roughly like T^6) of the electron and positron capture rates. At $t > 4\,{\rm ms}$, free neutrons and protons in the expanding matter partially recombine into α-particles ($\langle A_h \rangle = \sum_{Z\geqslant 2} AY / \sum_{Z\geqslant 2} Y \simeq 4$), thus giving rise to the α-effect and therefore a further increase of Y_e. The rate λ^* becomes larger than $\lambda_+ \simeq \lambda_{\nu_e}$ and approaches $(\lambda_{\bar{\nu}_e} + \lambda_{\nu_e})/2$ of material dominated by α-particles.

For trajectory 486857 (Fig. 4), at the initial density $\rho_{\rm eq}$, the mass element is characterised by a low temperature $T < 10^{10}$ K and consequently is composed of heavy nuclei $\langle A_h \rangle \simeq 120$ typical of the low values of $Y_e \simeq 0.1$ in the outer NS crust. The fast e^- and (anti)neutrino capture rates lead to a rapid increase of Y_e, but all these rates are comparable and Y_e fluctuates wildly. The mass element is then subject to a new compression phase that sets in at $t \simeq 1.5$ ms, and the corresponding high temperatures ($T \gtrsim 10^{11}$ K) photodissociate the matter into free nucleons. It should be noted that during this recompression episode, the higher densities cause neutrinos to become trapped again, for which reason the application of Eqs. (9,10) remains problematic and highly schematic. However, at these high-density, high-temperature conditions, electron captures dominate and re-neutronize the material until they are counterbalanced by positron captures, whose rate increases dramatically to achieve weak equilibrium with the electron captures. During the subsequent expansion phase (at $t > 2\,{\rm ms}$), Y_e rises gradually until

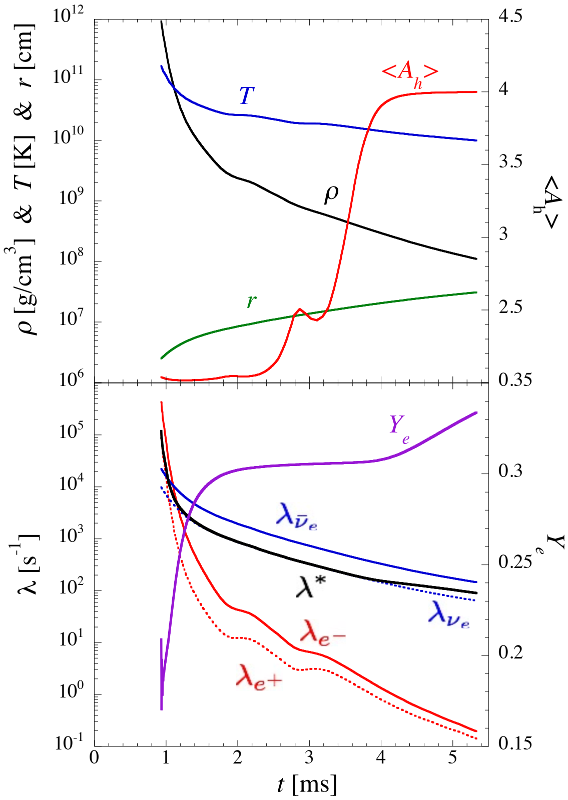

Figure 3. (Color online). *Upper panel*: Time evolution of temperature, density, radius, and mean atomic mass of nuclei heavier than protons, $\langle A_h \rangle = \sum_{Z\geqslant 2} AY / \sum_{Z\geqslant 2} Y$, between $\rho_{\rm eq}$ and $\rho_{\rm net}$ for trajectory 400720. *Lower panel*: Analogue for the electron (anti)neutrino, electron and positron capture rates, and for λ^* (Eq. 6) and the electron fraction. The (anti)neutrino properties correspond to Case 1. The late-time increase of Y_e is caused by the α-effect, which does not asymptote to a terminal value until the network is started. Y_e continues to evolve subsequently during the nucleosynthesis because of β-decays.

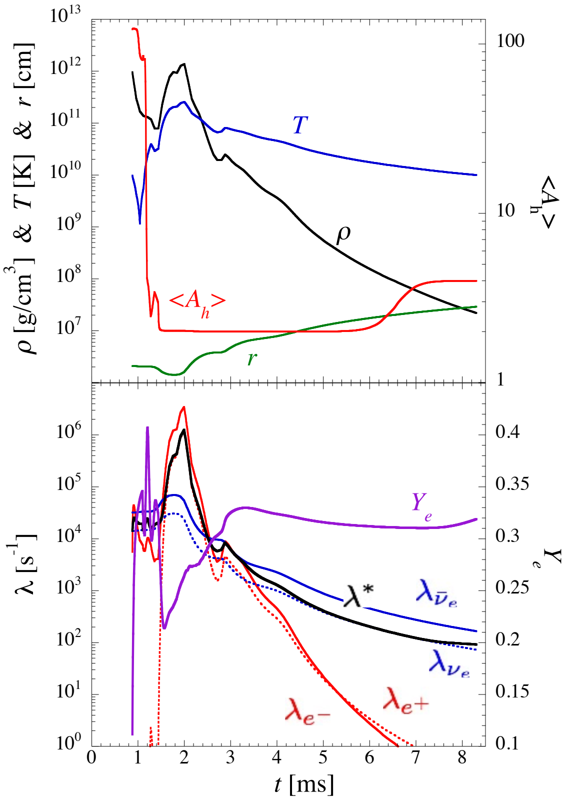

Figure 4. (Color online). Same as Fig. 3, but for trajectory 486857.

(anti)neutrino absorptions take over to push Y_e towards its asymptotic value of $Y_e^{\nu\infty} \simeq 0.31$ (at $t \sim 6$ ms). With decreasing temperatures, the α-effect finally becomes responsible for a late increase of Y_e at $t \gtrsim 7.5$ ms.

3.2 Y_e distributions

Six different cases are studied to estimate the impact of electron and positron captures as well as electron (anti)neutrino absorption on the ejecta mass distribution as function of Y_e. In the first case, weak interactions of free nucleons are not allowed. In the second case, electron and positron captures are turned on, but not (anti)neutrino absorptions. In the remaining four cases, both electron/positron captures as well as (anti)neutrino captures are switched on, with the (anti)neutrino properties being defined by Cases 1–4. For these six cases, the resulting Y_e distributions at density $\rho_{\rm net}$ are shown in Fig. 5.

In the first case without weak interactions of free nucleons below $\rho_{\rm eq}$ (upper left panel of Fig. 5), the Y_e distribution at $\rho_{\rm net}$ is identical to the one given at the initial density $\rho_{\rm eq}$. This case, however, differs from the standard case we considered previously (Goriely et al. 2011; Bauswein et al. 2013; Goriely et al. 2013; Just et al. 2015) in two aspects: First, we start our calculations of weak interactions at density $\rho_{\rm eq} = 10^{12}\,{\rm g\,cm^{-3}}$ with β-equilibrium distributions of electrons, positrons and neutrinos. This shifts and broadens the Y_e distribution from previous values of <0.1 to a wider range between 0 and ~0.3. Second, no temperature post-processing is performed here. The initial temperatures of the trajectories are significantly higher than those deduced from the post-processing applied in our previous studies.

As visible in Fig. 5, lower left panel, the Y_e distribution at density $\rho_{\rm net}$ is significantly affected by $e^{\pm}$-captures between $\rho_{\rm eq}$ and $\rho_{\rm net}$, although some low-Y_e ($\lesssim 0.2$) ejecta are left. Dominant parts of the ejecta are now found at Y_e values between 0.3 and 0.4. When switching on neutrino absorptions, for any of the Cases 1–4 the asymptotic values of $Y_e^{\nu\infty}$ are approached, and further enhancement by the α-effect produces peaks of the mass distributions in a range of Y_e values between 0.2 and 0.5. The peak values depend sensitively on the adopted neutrino properties. Cases 1 and 4 lead to rather similar Y_e distributions, owing to the fact that the neutrino properties are broadly comparable.

These distributions also depend sensitively on the temperature. When the temperature along the trajectory is ar-

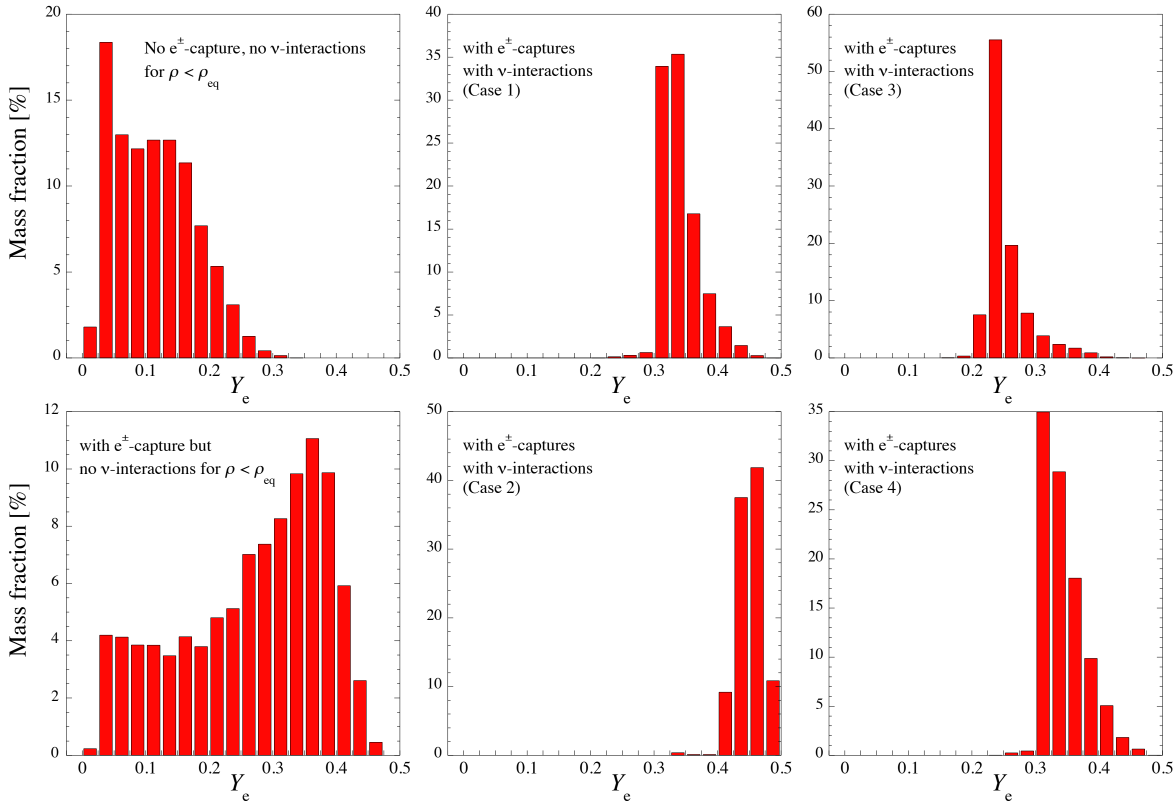

Figure 5. (Color online). Histograms of fractional mass distributions of the $4.9 \times 10^{-3} M_{\odot}$ of matter ejected in our 1.35–1.35$M_{\odot}$ NS-NS merger model as functions of Y_e at density $\rho_{\rm net}$, assuming that no weak interactions of free nucleons take place below $\rho_{\rm eq}$ (upper left), that only electron and positron captures affect the Y_e evolution for $\rho < \rho_{\rm eq}$ (lower left), and including electron and positron captures as well as (anti)neutrino captures at $\rho < \rho_{\rm eq}$ (Case 1: upper centre; Case 2: lower centre; Case 3: upper right; Case 4: lower right).

tificially increased or decreased by factors of 3, rather different results are obtained, as shown in Fig. 6, using the (anti)neutrino properties of Case 1. As before we start the expansion evolution at $\rho_{\rm eq}$ with the Y_e mass distribution shown in the upper left panel of Fig. 5. Reduced temperatures diminish the presence of positrons and thus favor electron captures compared to positron captures. Moreover, lower temperatures also lead to a faster freeze-out of $e^{\pm}$ captures during the ejection of the mass elements. Without neutrino and antineutrino absorptions, lower temperatures therefore tend to neutronize the ejecta for $\rho < \rho_{\rm eq}$ and the mass distribution becomes more narrow and is shifted to lower values in the range of $0 < Y_e \lesssim 0.1$ (Fig. 6, upper left panel). Including neutrino and antineutrino absorptions, reduced temperatures have the opposite effect in pushing the mass distribution to higher values of Y_e (with a peak above 0.4) compared to the standard-temperature result for Case 1 in Fig. 5 (upper right panel, with a peak of the distribution between $Y_e = 0.2$ and 0.3). This behavior can be understood by the efficient recombination of free nucleons to α particles and heavy nuclei, which strengthens the heavy-nuclei (α) effect so that the peak of the distribution wanders to $Y_e \simeq 0.45$. On the other side, increased temperatures reduce the electron degeneracy and thus allow for the presence of higher positron densities, thus enhancing positron captures on neutrons. In addition, $e^{\pm}$ captures continue for a longer period of time along the ejecta trajectories. Without (anti)neutrino absorption, these effects shift the Y_e mass distribution from the initial one at $\rho_{\rm eq}$ (upper left panel of Fig. 5) towards higher values of Y_e. This shift is stronger for more slowly expanding mass elements and weaker when the expansion is very fast. Correspondingly, the mass distribution versus Y_e at $\rho_{\rm net}$ is very broad and stretches from $\sim$0.03 up to a very pronounced maximum close to 0.5, because the $e^{\pm}$ capture equilibrium at high-entropy conditions favors symmetric conditions with respect to neutrons and protons. Taking into account (anti)neutrino absorption prevents this dramatic shift towards $Y_e \sim 0.5$, because at large distances neutrino captures dominate $e^{\pm}$ absorptions and therefore Y_e asymptotes to values around $Y_e^{\nu\infty}$ ($\simeq 0.31$ for Case 1, lower right panel of Fig. 6). Since the high temperatures favor nucleons and suppress the early formation of α particles and heavier nuclei, the influence of the α effect is clearly weaker than in the case of reduced temperatures (compare lower and upper right panels of Fig. 6). As mentioned above, our calculations with varied temperatures are not consistent with the initial Y_e distributions used at a density of $\rho_{\rm eq}$, because these distributions are calculated for the original ejecta temperatures provided by the hydrodynamic NS-NS merger model. However, Fig. 6 demonstrates that asymptotic values determined by neutrino capture equilibrium and influenced by the α (heavy-nuclei) effect are reached for most of the tra-

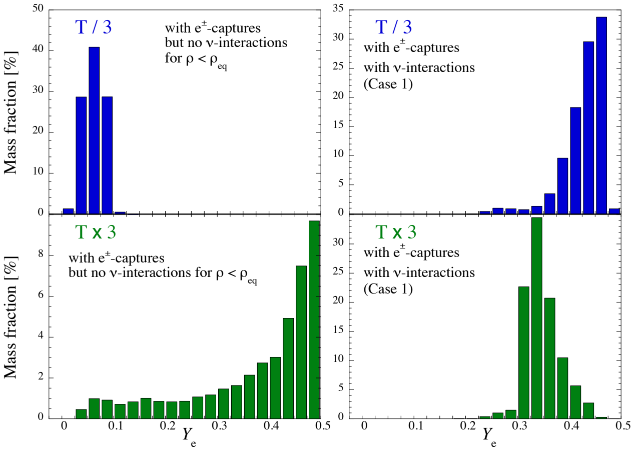

Figure 6. (Color online). Histograms of fractional mass distributions as functions of Y_e at density $\rho_{\rm net}$ for $e^{\pm}$ captures exclusively at $\rho < \rho_{\rm eq}$ (left) and including electron, positron captures as well as (anti)neutrino captures during the evolution from $\rho_{\rm eq}$ to $\rho_{\rm net}$ (Case 1; right), when the temperatures are decreased (upper panels) or increased (lower panels) artificially by factors of 3.

jectories. The final Y_e values can therefore be expected to mostly have lost the memory of the initial conditions at $\rho_{\rm eq}$. Correspondingly, when neutrino absorptions are included, the final mass distributions of Y_e (at $\rho_{\rm net}$) are considerably more narrow than the relatively broad distribution of initial Y_e values before the expansion from $\rho_{\rm eq}$ to $\rho_{\rm net}$ (compare the right panels of Fig. 6 with the upper left panel of Fig. 5).

4 R-PROCESS NUCLEOSYNTHESIS

At densities $\rho < \rho_{\rm net}$, the abundance evolution is followed by a full reaction network (for more details, see Goriely et al. 2011; Bauswein et al. 2013; Goriely et al. 2013; Just et al. 2015), which in contrast to earlier studies includes now also the weak interactions of free nucleons as detailed in Sect. 2. The final abundance distributions are shown in Fig. 7 for the same six different cases discussed in Sect. 3.2 and displayed in Fig. 5, namely for a case without weak interactions of free nucleons below $\rho_{\rm eq}$, a case including $e^{\pm}$-captures but without (anti)neutrino absorption reactions, and four cases where both $e^{\pm}$- and (anti)neutrino captures are taken into account at $\rho < \rho_{\rm eq}$ (Cases 1–4 for the ν properties).

Because of its low-Y_e distribution, the case neglecting β-interactions gives rise to an elemental abundance distribution similar to the one obtained in our previous studies (Goriely et al. 2011; Bauswein et al. 2013; Goriely et al. 2013; Just et al. 2015). It is characterized by the production of essentially only $A > 140$ nuclei through several loops of fission recycling. When $e^{\pm}$-captures on free nucleons are switched on, some low-Y_e ($\lesssim 0.2$) material can still lead to nucleosynthesis with fission recycling and a significant production of the third r-process peak, but the higher-Y_e (0.3–0.4) matter can now also contribute to the production of $90 \leqslant A \leqslant 140$ nuclei with a strong second $N = 82$ peak.

When (anti)neutrino captures are included, too, nucleosynthesis with fission recycling does not take place any longer, but the final abundance distribution still resembles the one in the solar system fairly well. A significant amount of $50 \leqslant A \leqslant 90$ nuclei can now also be produced in addition to the $A > 90$ r-nuclei, especially for (anti)neutrino properties corresponding to Case 2, as shown in Fig. 8. In this case, important element production around ^{60}Ni is obtained, originating from ejected mass elements with $Y_e \gtrsim 0.45$.

Without β-interactions below $\rho_{\rm eq}$, about 90% of the ejected material is found to be r-process rich. If $e^{\pm}$-captures on nucleons are switched on, the material is made of 76% r-process nuclei, and when (anti)neutrino captures are effective, too, we find that 45% of the ejected matter is made of r-nuclei in Case 1, only 1.9% in Case 2, 67% in Case 3 and 40% in Case 4. In the last four cases, a significant part of the material is made of α-particles ($\sim$ 22% in Cases 1 and 4, 50% in Case 2, and 17% in Case 3), and the remaining part consists of $50 \leqslant A \leqslant 70$ nuclei (see Fig. 8). Despite the rather robust production of a solar-like distribution of r-nuclei, the absolute and relative amounts of r-material vary strongly from case to case, sensitively depending on the neutrino exposure of the ejecta as determined by the assumed properties of the neutrino emission. Neutrino properties corresponding to Case 2 yield a total amount of ejected r-material that is significantly smaller than for the other three sets of neutrino properties.

The total, mass-averaged nuclear energy-release rate that is available for heating the ejecta per unit of mass, the average temperature of the ejecta, and the average atomic mass number of the ejected abundance yields are plotted as functions of time for our six studied cases in Fig. 9. After some 10 s and up to nearly one day, the energy release rates of all cases are fairly similar except for the treatment of neutrinos and β-interactions according to Case 2. In this case, the large electron fractions of the ejecta favor the production of light elements and only a small amount ($\sim$ 2%) of the ejecta material consists of r-process nuclei (Fig. 8) and is therefore subject to fast β-decays. At late times, typically after one day, an additional source of energy is found from the α-decay of long-lived heavy nuclei that can only be significantly produced when no β-interaction of nucleons are included below $\rho_{\rm eq}$. Despite the considerable differences of the nuclear energy-release rates at early times, the cooling evolution as measured by the mass-averaged temperatures is rather similar in all cases.

The time evolution of the average nuclear mass number of the ejected material clearly shows that only without β-interactions of free nucleons a significant amount of fissile nuclei can be produced with $\langle A \rangle$ reaching values up to 170, which is slightly below the value of about 200 obtained when the Y_e distribution of the inner crust of a cold NS is considered as initial state (see, in particular, Goriely et al. 2011). The sequence of decreasing values of $\langle A \rangle$ follows basically the hierarchy of increasing values of the mean electron fraction, namely $\langle Y_e \rangle = 0.11$ when β-interactions are ignored, $\langle Y_e \rangle = 0.27$ when only $e^{\pm}$-captures are taken into account, and $\langle Y_e \rangle = 0.25$, 0.34, 0. 35, 0.45 in the Cases 3, 1, 4 and 2, respectively. The only (slight) inversion is obtained for the calculation with only $e^{\pm}$-captures, because in this case the Y_e distribution is very wide (Fig. 5, lower left panel) and the significant amounts of low-Y_e ($\sim 0.05 - 0.15$) material contribute to the production of heavy nuclei which increase the average nuclear mass number $\langle A \rangle$.

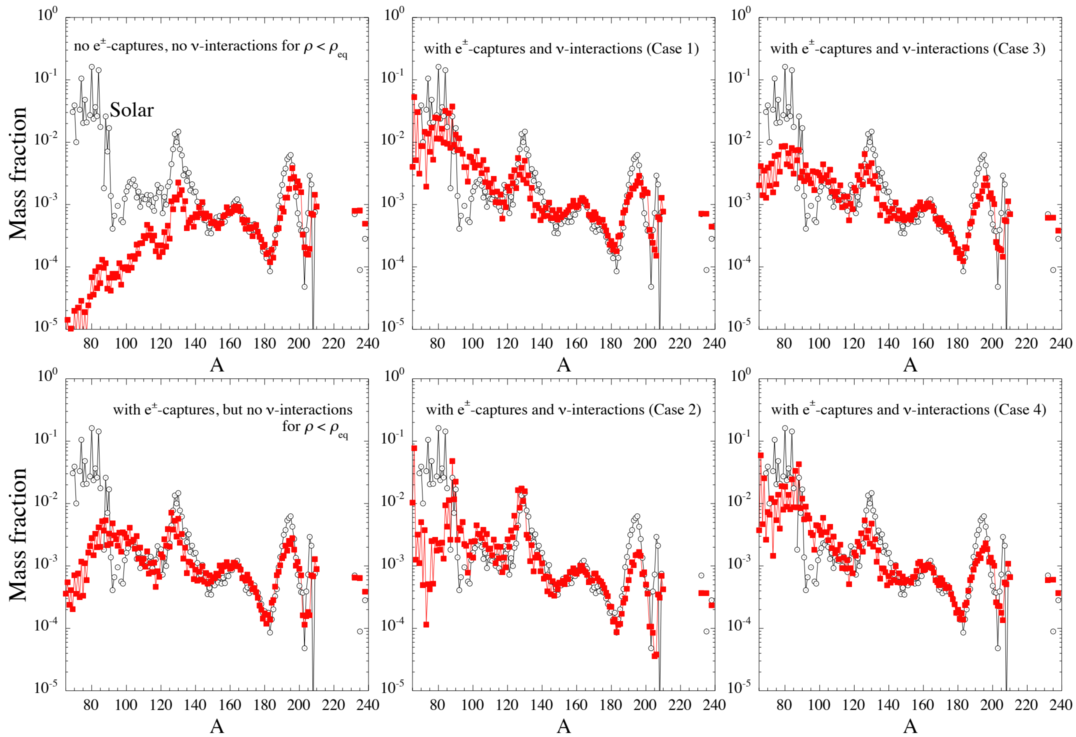

Figure 7. (Color online). Abundance distributions of the $4.9 \times 10^{-3} M_{\odot}$ of material ejected in our 1.35–1.35$M_{\odot}$ NS-NS merger model, assuming that no weak interactions of free nucleons take place at $\rho < \rho_{\mathrm{eq}}$ (upper left), only electron and positron captures happen below ρ_{eq} (upper right), and electron and positron captures as well as (anti)neutrino captures affect the Y_e evolution for $\rho < \rho_{\mathrm{eq}}$ (Case 1: upper centre; Case 2: lower centre; Case 3: upper right; Case 4: lower right). The abundance distributions are normalized to the solar r-abundance distribution (open circles) in the rare-earth peak ($A = 165$) region.

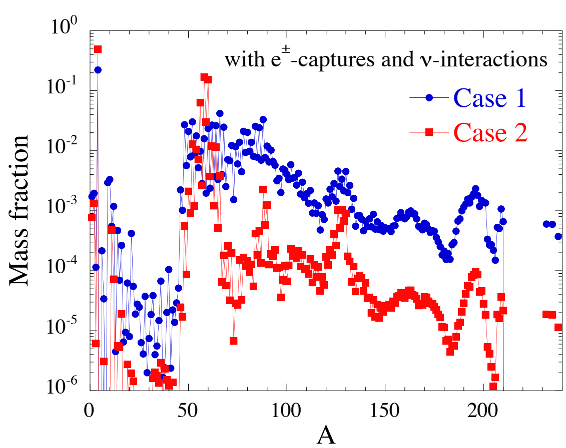

Figure 8. (Color online). Mass fraction as a function of the atomic mass for the matter ejected by our 1.35–1.35$M_{\odot}$ NS merger model, including electron, positron as well as (anti)neutrino captures for Cases 1 and 2 of the neutrino properties.

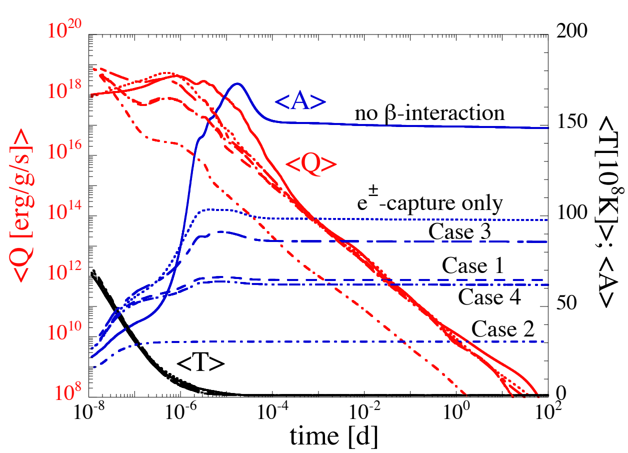

Figure 9. (Color online). Time evolution of the total radioactive heating rate per unit mass, $\langle Q \rangle$ (red), mass number $\langle A \rangle$ (blue), and temperature $\langle T \rangle$ (black), all mass-averaged over the ejecta, for the 1.35–1.35$M_{\odot}$ NS merger. The solid lines correspond to the case without β-interactions of free nucleons at $\rho < \rho_{\mathrm{eq}}$, the dotted lines to the case where only $e^{\pm}$-captures are taken into account, the dashed lines to the case where $e^{\pm}$ and (anti)neutrino captures for neutrino properties according to Case 1 are included, the dash-dot lines for neutrinos according to Case 2, the long-dash-dot lines correspond to Case 3, and the double-dash-dot lines to Case 4.

5 SUMMARY AND CONCLUSIONS

In this paper we reported the results of a parametric study to investigate how β-interactions of free nucleons can affect the Y_e evolution and mass distribution in NS merger ejecta

and the corresponding nucleosynthesis. To this end we used the temperature-density trajectories of a large set of mass elements representing the $\sim 5 \times 10^{-3}\,M_\odot$ of matter ejected in a relativistic merger simulation of a symmetric $1.35M_\odot$-$1.35M_\odot$ NS binary with the non-zero temperature DD2 nuclear equation of state. Using the total lepton number provided by our NS-NS merger simulation, we assume matter to be in β equilibrium at the temperature of the hydrodynamical model and a fiducial density of $\rho_{\rm eq} = 10^{12}\,{\rm g\,cm^{-3}}$. These conditions define the starting points of our post-processing of the composition histories of the considered ejecta elements, for which we take into account electron and positron captures as well as electron neutrino and antineutrino absorption on free neutrons and protons. Below a density $\rho_{\rm net}$, where the temperature has decreased to $10^{10}\,{\rm K}$ (or the neutron drip density, if matter below $\rho_{\rm eq}$ remains cooler than $10^{10}\,{\rm K}$) the full network calculation is applied instead of nuclear statistical equilibrium. Our description of weak interactions of free nucleons includes weak magnetism and recoil corrections according to Horowitz & Li (1999) and Pllumbi et al. (2014). Avoiding the complications of treating neutrino transport, we simply use exemplary data from publications for prescribing the neutrino luminosities and mean energies needed to compute the neutrino absorption rates in our parametric approach ("Cases 1–4"). This elementary prescription also accounts for the still large uncertainties of the model predictions for the neutrino emission and its directional asymmetries in the generically three-dimensional merger scenario.

Our modeling strategy follows the spirit of previous, numerous parametric investigations of nucleosynthesis in the neutrino-driven wind of newly formed neutron stars in supernovae (e.g., McLaughlin et al. 1996; Meyer et al. 1998; Arnould et al. 2007; Pllumbi et al. 2014, and references therein) and of accretion tori around black holes as remnants of compact object mergers (e.g., Surman & McLaughlin 2005; Surman et al. 2008; Wanajo & Janka 2012; Caballero et al. 2012). In particular, we track in detail the charged-current β-interactions of neutrinos with free nucleons, which determine the evolution of the electron fraction outside of the neutrino-trapping regime, and employ a full set of trajectories that characterizes the conditions in dynamical ejecta from the merging phase of a representative binary neutron star. These conditions differ from proto-neutron star and accretion-torus winds not only concerning the range of entropies. The ejecta, especially, possess much faster expansion velocities, which for the bulk of the matter can be 25–50% of the speed of light, for some fraction of the ejecta even faster, whereas neutrino-driven proto-neutron star winds have typical velocities of 3–7% of the speed of light (e.g., Arcones et al. 2007), neutrino-driven winds from massive neutron stars as relics of NS mergers may achieve expansion velocities up to 8–10% of the speed of light (Perego et al. 2014), and the main mass of neutrino-driven outflows from BH-accretion tori can reach 10–20% of the speed of light (Just et al. 2015). The correspondingly shorter expansion time scales of dynamical merger ejecta can enable a strong r-process even for moderately low Y_e.

Our calculations confirm recent results of Wanajo et al. (2014) that solar-like r-process abundances are produced in dynamical NS merger ejecta even when β-reactions of free nucleons are taken into account and lead to a significant increase of the average electron fraction. In contrast to previous works, where charged-current neutrino-nucleon interactions were ignored, however, also nuclei with mass numbers $A < 140$ are ejected in larger amounts.

In detail, our results can be summarized by the following points:

- Ignoring β-interactions at densities $\rho < \rho_{\rm eq}$, we confirm our previous results of Goriely et al. (2011); Bauswein et al. (2013); Goriely et al. (2013); Just et al. (2015) that almost exclusively r-nuclei in the regime $A \gtrsim 140$ are produced, in spite of a moderate increase of the average ejecta Y_e associated with the assumption of β-equilibrium at density $\rho_{\rm eq}$ instead of our previous use of electron fractions of cold neutron star crust matter.
- Positron and electron-neutrino captures, enhanced by weak magnetism corrections (which increase the absorption cross section of ν_e and reduce that of $\bar{\nu}_e$) and supported by the α effect, lead to a shift of the average ejecta Y_e towards higher values when matter expands downwards from an initial density of $\rho_{\rm eq} = 10^{12}\,{\rm g\,cm^{-3}}$.
- Captures of $e^\pm$ cause a wide spread of the Y_e mass distribution, reaching from values of $Y_e \ll 0.1$ up to 0.4–0.5. This reflects the wide range of thermodynamic conditions of the ejecta at $\rho_{\rm eq}$ with ejecta trajectories that describe cool as well as hot conditions. Absorption processes of ν_e and $\bar{\nu}_e$ take over when the temperature of the expanding matter has fallen to low values where $e^\pm$ absorptions become ineffective. These (anti)neutrino captures tend to push Y_e towards the asymptotic value $Y_e^{\nu\infty}$ for ν_e-$\bar{\nu}_e$ capture equilibrium. The corresponding Y_e mass distributions (at $\rho_{\rm net}$, where the full network calculation was started) are rather narrow in all cases, with a spread of Y_e values of only 0.1–0.15. The mean values of the distributions, however, vary between $\sim$0.25 and $\sim$0.45, depending on the relative size of the ν_e and $\bar{\nu}_e$ luminosities. The latter are highly uncertain and variable and are sensitive to the binary-parameter dependent merger dynamics, the nuclear equation of state, and the still not well determined directional asymmetries of the neutrino emission.
- In the presence of β-interactions of free nucleons the temperature also plays an important role for the Y_e evolution of the ejecta. It is another aspect of the hydrodynamical merger models that depends on the system properties and the detailed ejection dynamics (which differ between different ejecta components) and can be numerically problematic, because resolution and numerical/artificial viscosity can have an influence on the accuracy of the determination of the thermal conditions. Lower temperatures reduce the effects of $e^\pm$ captures but increase the importance of the α effect (thus pushing the average Y_e closer to 0.5), whereas higher temperatures enhance $e^\pm$ captures but nevertheless have little influence on the final Y_e distribution at $\rho_{\rm net}$, for which the asymptotic value of ν_e-$\bar{\nu}_e$ capture equilibrium is more relevant than the initially fast $e^\pm$ captures.
- In all investigated model cases, the production of heavy r-process matter with strong second and third abundance peaks and a near-solar distribution in the rare-earth region is a robust outcome. However, in contrast to previous results where weak interactions of free nucleons were ignored, also considerable amounts of matter are synthesized to $A < 140$ nuclei. The strength of the production of $A \lesssim 90$–100 ma-

terial is sensitive to the neutrino-emission properties that determine the (anti)neutrino absorption. In extreme cases where Y_e gets close to 0.5, significant amounts of iron-group nuclei ($A \sim 50$–60) can be ejected. The relative fraction of heavy r-process matter (from the second peak upward) in the ejecta therefore varies dramatically between the different investigated cases of neutrino-emission conditions and spans a range from more than 75% down to just 2%.

We emphasize that our parametric approach is highly simplified and ignores important neutrino-transport effects like the exact spectral distribution of the neutrino fluxes, the direction dependence of the neutrino emission and corresponding precise radial dilution function, and the time evolution of the neutrino emission relative to the ejection time of the matter. Nevertheless, our results, in support of those of Wanajo et al. (2014) and Sekiguchi et al. (2015), have important consequences for the further exploration of the nucleosynthesis connected to compact binary mergers and the discussion of astrophysical implications. In fact, they demand a major revision of the current picture of r-process production in such events.

In view of our results it is obvious that a proper treatment of the neutrino physics, in particular of the neutrino irradiation of the ejected material, is essential for making quantitative predictions of the elemental yields and especially of the total mass of r-process material that is thrown out by the dynamical merger ejecta. Approximations like the ones used in our study can be satisfactorily removed only when ultimately detailed, three-dimensional neutrino transport is consistently included in the hydrodynamical simulations.

Our study suggests that the relative contributions of matter with $A \lesssim 90$, $90 \lesssim A \lesssim 140$ and $A \gtrsim 140$ are likely to depend strongly on the binary properties and even the direction of mass ejection, in addition to the equation of state dependence that was found for the electron-fraction distribution in the recent work of Sekiguchi et al. (2015). Different from expectations so far, this means that symmetric or nearly symmetric binary NS mergers could exhibit a significantly different ejecta composition than highly asymmetric NS-NS mergers and NS-BH mergers, in which the NS is disrupted before it can be swallowed by the BH. In the last two cases the lower-mass component develops an extended tidal tail, from which considerable amounts of cold, unshocked matter can be centrifugally ejected before the neutrino luminosities rise high and thus before neutrino exposure of these ejecta plays an important role. In such a situation the ejecta will not only be expelled highly anisotropically but will also carry a far dominant fraction of the mass in the form of $A \gtrsim 140$ nuclei as predicted in previous studies (e.g., Goriely et al. 2011; Bauswein et al. 2013; Goriely et al. 2013; Just et al. 2015). In contrast, in symmetric or nearly symmetric NS mergers the contribution of $A \lesssim 140$ material will be higher. If the merger remnant collapses to a BH on a millisecond time scale, neutrino exposure of the ejecta may be avoided, but the broad Y_e distribution caused by $e^{\pm}$ captures will allow for the production of $A > 90$ nuclei with a strong second $N = 82$ peak. If the merger remnant remains transiently or permanently stable, neutrino exposure of the dynamically expelled matter becomes important, enabling a higher production of $A \lesssim 90$ species. For extreme cases of a luminous ν_e flux, the ejecta might then even be dominated by iron-group nuclei including radioactive nickel isotopes. In particular, however, the exact composition and the relative fraction of high-mass and low-mass species could depend on the direction of the mass ejection. If most of the neutrino flux is emitted to the polar directions due to the rotational deformation of the merger remnant, matter expelled near the equatorial plane will receive less neutrino exposure in addition to its potentially faster escape. This will allow for more neutron-rich conditions close to the equator whereas polar ejecta may contain more proton-rich contributions. Future, more complete merger models with neutrino transport will have to clarify these possibilities.

Since the photon opacity, κ, of the expanding gaseous ejecta is strongly dependent on the presence of high-opacity, complex ions (the lanthanides; Barnes & Kasen 2013; Kasen et al. 2013; Tanaka & Hotokezaka 2013; Tanaka et al. 2014), the relative contribution of trans-iron elements to the ejecta will have a severe impact on the peak luminosity, $L_{\rm peak} \propto \kappa^{-1/2}$, peak time, $t_{\rm peak} \propto \kappa^{1/2}$, and the effective peak temperature, $T_{\rm peak} \propto \kappa^{-3/8}$, of the electromagnetic transient that is expected from the radioactively heated, dynamical ejecta cloud ("macronova" or "kilonova", Li & Paczyński 1998; Kulkarni 2005; Metzger et al. 2010; Roberts et al. 2011; Goriely et al. 2011). The current picture of merger-type and remnant-type dependent redder (near-infrared) or bluer emission (Metzger & Fernández 2014; Perego et al. 2014) and in particular of the envisioned late-time infra-red radiation component from the dynamical ejecta (Kasen et al. 2014) might require revision or extension in view of our results.

Finally, it is evident that the strong impact of neutrinos on the neutron-to-proton ratio and the nuclear composition of the dynamic merger ejecta must move neutrino oscillations into the focus of interest. It will be necessary to study the effects of collective neutrino oscillations (see, e.g., Duan et al. 2010, for a review) with similiar intensity as this subject currently receives in the context of the neutrino emission from newly born neutron stars in supernovae.

ACKNOWLEDGMENTS

SG acknowledges financial support from FNRS (Belgium). At Garching, this research was supported by the Max-Planck/Princeton Center for Plasma Physics (MPPC) and by the Deutsche Forschungsgemeinschaft through the Cluster of Excellence EXC 153 "Origin and Structure of the Universe" (http://www.universe-cluster.de). AB is a Marie Curie Intra-European Fellow within the 7th European Community Framework Programme (IEF 331873). We are also grateful for computing time at the Rechenzentrum Garching (RZG).

REFERENCES

Arcones A., Janka H.-T., Scheck L., 2007, A&A, 467, 1227
Arnould M., Goriely S., Takahashi K., 2007, Phys. Rep., 450, 97
Barnes J., Kasen D., 2013, ApJ, 775, 18
Bauswein A., Goriely S., Janka H.-T., 2013, ApJ, 773, 78

Burrows A., 2013, Reviews of Modern Physics, 85, 245
Caballero O.L., McLaughlin G.C., Surman R., 2012, ApJ, 745, 170
Dessart L., Ott C. D., Burrows A., Rosswog S., Livne E., 2009, ApJ, 690, 1681
Duan H., Fuller G.M., Qian Y.-Z., 2010, ARNPS 60, 569
Freiburghaus C., Rosswog S., Thielemann F.-K., 1999, ApJ, 525, L121
Goriely S., Bauswein A., Janka H.-T., 2011, ApJL, 738, L32
Goriely S., Sida J.-L., Lemaître J.-F., Panebianco S., Dubray N., Hilaire S., Bauswein A., Janka H.-T., 2013, Phys. Rev. Lett., 111, 242502
Hempel M., Schaffner-Bielich J., 2010, Nucl. Phys. A, 837, 210
Horowitz C.J., Li G., 1999, Phys. Rev. Lett., 82, 5198
Hotokezaka K., Kiuchi K., Kyutoku K., Okawa H., Sekiguchi Y.-i., Shibata M., Taniguchi K., 2013, Phys. Rev. D, 87, 024001
Janka H.-T., 2012, Ann. Rev. Nuc. Part. Science, 62, 407
Just O. , Bauswein A., Ardevol Pulpillo R., Goriely S., Janka H.-T., 2015, MNRAS, 448, 541
Kasen D., Badnell N.R., Barnes J., 2013, ApJ, 774, 25
Kasen D., Fernández R., Metzger B.D., arXiv:1411.3726 (astro-ph)
Komiya Y., et al., 2014, ApJ, 783, 132
Korobkin O., Rosswog S., Arcones A., Winteler C., 2012, MNRAS, 426, 1940
Kulkarni S.R., 2005, arXiv:astro-ph/0510256
Li L.-X., Paczyński B., 1998, ApJL, 507, L59
Matteucci F., et al., 2014, MNRAS, 438, 2177
McLaughlin G.C., Fuller G.M., Wilson J.R., 1999, ApJ, 472, 440
Mennekens N., Vanbeveren D., 2014, A&A, 564, A134
Metzger B.D., Martinez-Pinedo G., Darbha S., et al., 2010, MNRAS, 406, 2650
Metzger B.D., Fernández R., 2014, MNRAS, 441, 3444
Meyer B.S., McLaughlin G.C., Fuller G.M.,1998, Phys. Rev. C, 58, 3696
Nishimura N., Takiwaki T., Thielemann F.-K., 2015, arXiv:1501.06567
Perego A., Rosswog S., Cabezón R. M., Korobkin O., Käppeli R., Arcones A., Liebendörfer M., 2014, MNRAS, 443, 3134
Pllumbi, E., et al., 2014, arXiv1406.2596
Roberts L.F., Kasen D., Lee W.H., Ramirez-Ruiz E., 2011, ApJL, 736, L21
Roederer I.U., 2011, ApJL, 732, L17
Roederer I.U., et al., 2012, ApJS, 203, 27
Rosswog S., Liebendörfer M., 2003, MNRAS, 342, 673
Rosswog S., Liebendörfer M., Thielemann F.-K., Davies M.B., Benz W., Piran T., 1999, A&A, 341, 499
Ruffert M., Janka H.-T., 1999, A&A, 344, 573
Ruffert M., Janka H.-Th., 2001, A&A, 380, 544
Ruffert M., Janka H.-T., Schaefer G., 1996, A&A, 311, 532
Sekiguchi Y., Kiuchi K., Kyutoku K., Shibata M., 2015, arXiv:1502.06660
Shen S., Cooke R., Ramirez-Ruiz E., Madau P., Mayer L., Guedes J., 2014, arXiv:1407.3796
Surman R., McLaughlin, G.C., 2005, ApJ, 618, 397
Surman R., McLaughlin, G.C., Ruffert M., Janka H.-T., Hix W.R., 2008, ApJL, 679, L117
Takahashi K., El Eid M.F., Hillebrandt W., 1978, A&A, 67, 185
Tanaka M., Hotokezaka K., 2013, ApJ, 775, 113
Tanaka M., Hotokezaka K., Kyutoku K., et al., 2014, ApJ, 780, 31
Typel S., Röpke G., Klähn T., Blaschke D., Wolter H.H., 2010, Phys. Rev. C, 81, 015803
van de Voort F., Quataert E., Hopkins P. F., Keres D., Faucher-Giguere C.-A., 2015, MNRAS, 447, 140
Vangioni E., Goriely S., Daigne F., François P., Belczynski K., arXiv:astro-ph/1409.2462
Wanajo S., Janka H.-Th., & Müller, B., 2011, ApJL, 726, L15
Wanajo S., Janka H.-Th., 2012, ApJ, 746, 180
Wanajo S., et al., 2014, ApJ, 789, L39
Wehmeyer B., M. Pignatari M., Thielemann F.-K., 2015, arXiv: 1501.07749
Winteler C., Käppeli R., Perego A., et al., 2012, ApJL, 750, L22